IL-17–induced CXCL12 recruits B cells and induces follicle formation in BALT in the absence of differentiated FDCs

Henrike Fleige,[1] Sarina Ravens,[1] Georgios Leandros Moschovakis,[1] Jasmin Bölter,[1] Stefanie Willenzon,[1] Gerd Sutter,[2] Susanne Häussler,[3] Ulrich Kalinke,[4] Immo Prinz,[1] and Reinhold Förster[1]

[1]Institute of Immunology, Hannover Medical School, 30625 Hannover, Germany
[2]Institute for Infectious Diseases and Zoonoses, University of Munich LMU, 80539 Munich, Germany
[3]Institute of Molecular Bacteriology and [4]Institute for Experimental Infection Research, TWINCORE, Centre for Experimental and Clinical Infection Research, a joint venture between the Helmholtz-Centre for Infection Research and the Hannover Medical School, 30625 Hannover, Germany

Ectopic lymphoid tissue, such as bronchus-associated lymphoid tissue (BALT) in the lung, develops spontaneously at sites of chronic inflammation or during infection. The molecular mechanisms underlying the neogenesis of such tertiary lymphoid tissue are still poorly understood. We show that the type of inflammation-inducing pathogen determines which key factors are required for the formation and maturation of BALT. Thus, a single intranasal administration of the poxvirus modified vaccinia virus Ankara (MVA) is sufficient to induce highly organized BALT with densely packed B cell follicles containing a network of CXCL13-expressing follicular DCs (FDCs), as well as CXCL12-producing follicular stromal cells. In contrast, mice treated with *P. aeruginosa* (*P.a.*) develop BALT but B cell follicles lack FDCs while still harboring CXCL12-positive follicular stromal cells. Furthermore, in IL-17–deficient mice, *P.a.*-induced BALT largely lacks B cells as well as CXCL12-expressing stromal cells, and only loose infiltrates of T cells are present. We show that Toll-like receptor pathways are required for BALT induction by *P.a.*, but not MVA, and provide evidence that IL-17 drives the differentiation of lung stroma toward podoplanin-positive CXCL12-expressing cells that allow follicle formation even in the absence of FDCs. Taken together, our results identify distinct pathogen-dependent induction and maturation pathways for BALT formation.

CORRESPONDENCE
Reinhold Förster:
foerster.reinhold@mh-hannover.de

Abbreviations used: BALT, bronchus-associated lymphoid tissue; FDC, follicular DC; FRC, fibroblastic reticular cell; LT, lymphotoxin; MVA, modified vaccinia virus Ankara; *P.a.*, *Pseudomonas aeruginosa*.

Bronchus-associated lymphoid tissue (BALT) represents a major component of the larger network of mucosa-associated lymphoid tissues, which essentially contribute to the initiation and maintenance of protective immune responses against invading pathogens. BALT is defined as aggregations of immune cells in the lung, containing a follicle-like structure composed of B cells which is surrounded by parafollicular T cell areas (Randall, 2010). To be classified as BALT, such lymphoid aggregates have to be situated adjacent to a bronchus and next to a vein and an artery. Furthermore, BALT contains some myeloid cells, in particular DCs, a network of stromal cells, and, depending on its state of maturation, follicular DCs (FDCs) within the B cell follicles (Kocks et al., 2007; Halle et al., 2009; Randall, 2010). The formation of high endothelial venules and lymphatic vessels facilitates the recirculation of lymphocytes (Xu et al., 2003).

Although the lungs of naive mice (as well as adult humans) are typically devoid of BALT, pulmonary infection in mice with pathogens such as influenza virus (Moyron-Quiroz et al., 2004), murine herpesvirus 68 (Kocks et al., 2009), *Mycobacterium tuberculosis* (Kahnert et al., 2007), or modified vaccinia virus Ankara (MVA) (Halle et al., 2009) have been described to induce these tertiary lymphoid structures. Despite morphological

S. Ravens' present address is Dept. of Functional Genomics, Institut de Génétique et de Biologie Moléculaire et Cellulaire, CNRS UMR 7104, INSERM U964, Université de Strasbourg, Illkirch Cedex, 67404 Strasbourg, France.

The Rockefeller University Press $30.00
J. Exp. Med. 2014 Vol. 211 No. 4 643-651
www.jem.org/cgi/doi/10.1084/jem.20131737

The Journal of Experimental Medicine

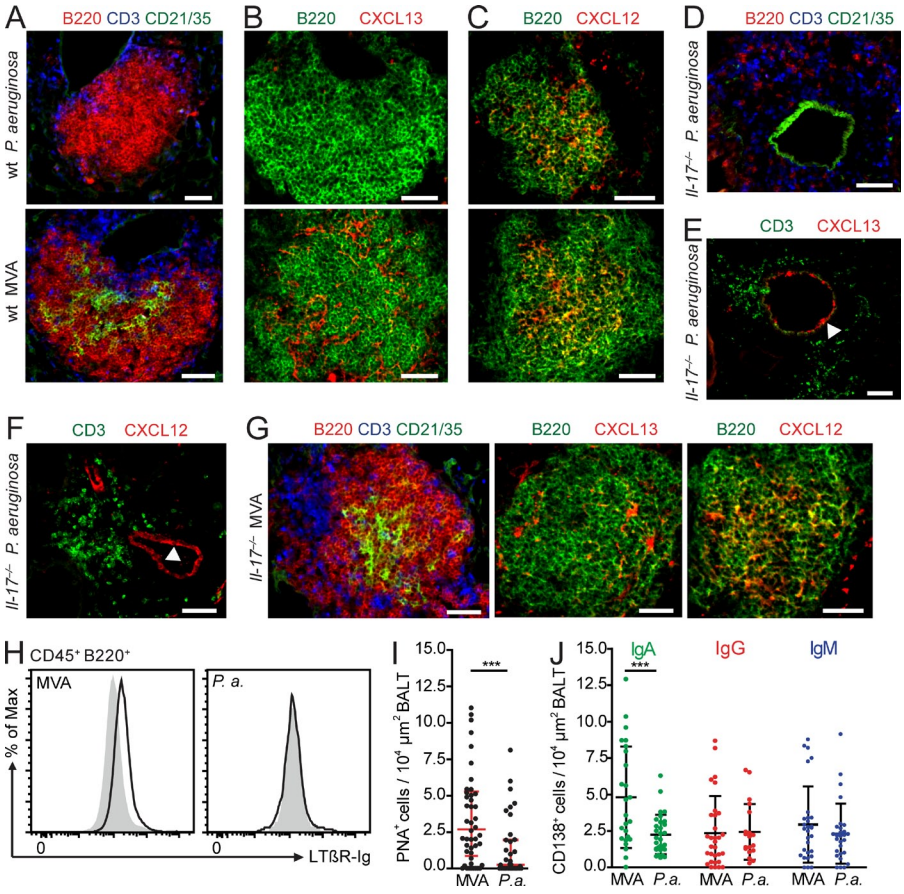

Figure 1. *P.a.*-induced BALT lacks FDCs and depends on IL-17. (A–G) Immunofluorescence microscopy of BALT in the lungs of 10–12-wk-old C57BL/6 WT (A–C) or C57BL/6 *Il17a/f*$^{-/-}$ (D–G) mice. 12 d after intranasal (i.n.) administration of heat-inactivated *P.a.* or intact MVA, frozen lung sections were stained with the antibodies indicated. Bars, 100 µm. Data are representative of two to four independent experiments with 9–16 WT and 7 *Il17a/f*$^{-/-}$ mice. Arrowheads in E and F indicate unspecific staining of vessels and bronchi that is also present in controls lacking primary antibodies. (H) Expression of LT$\alpha_1\beta_2$ (solid black line) on B220$^+$ cells from lungs of WT mice 8–12 d after i.n. administration of *P.a.* or MVA assessed by flow cytometry. Gray shaded histograms depict control staining with anti-human IgG only. Data are representative of two independent experiments with 3–4 mice analyzed per group. (I) Number of PNA$^+$ cells per 10^4 µm^2 BALT section area 12 d after *P.a.* or MVA administration. Data are derived from two independent experiments with 9 MVA-treated and 8 *P.a.*-treated WT mice. Error bars indicate median and IQR; ***, $P < 0.001$. (J) Number of IgA-, IgG-, and IgM-expressing CD138$^+$ plasma cells per 10^4 µm^2 BALT section area 12 d after *P.a.* or MVA administration. Data are derived from two independent experiments with 5 MVA-treated and 6 *P.a.*-treated WT mice. Error bars indicate mean and SD; ***, $P < 0.001$.

and functional similarities between lymph nodes and BALT, developmental pathways that control the formation and maintenance of the latter remain largely unknown. The development of lymph nodes requires the presence of lymphotoxin (LT) $\alpha_1\beta_2$-expressing lymphoid tissue inducer (LTi) cells (van de Pavert and Mebius, 2010) to stimulate the differentiation of stromal organizer cells, which in turn express lymphocyte-recruiting chemokines such as CXCL13 and CCL21. In contrast, induction of BALT and the presence of CXCL13- and CCL21-expressing cells within these structures seem to occur independently of LTi cells (Moyron-Quiroz et al., 2004), instead relying on DCs (Halle et al., 2009) expressing LT$\alpha_1\beta_2$ (GeurtsvanKessel et al., 2009).

The chemokine receptor CXCR4 is expressed on B cells and facilitates their efficacious migratory response toward its ligand CXCL12 (Okada et al., 2002). In combination with two other homeostatic chemokine receptors, CXCR5 and CCR7, CXCR4 is regulating the homing of B cells to Peyer's patches (Okada et al., 2002), but so far the functional relevance of the CXCL12–CXCR4 axis for B cell homing toward or follicle formation within BALT has not been addressed.

Recently, a model for BALT induction based on the repeated intranasal sensitization of newborn mice with LPS has been reported to be dependent on the production of IL-17 by T cells (Rangel-Moreno et al., 2011). At the same time, we demonstrated that the formation of MVA-induced BALT occurs completely independent of this cytokine (Fleige et al., 2012). Collectively, these data strongly suggested that at least two different signaling pathways can independently control BALT induction.

In the present study, we used MVA and *P. aeruginosa* (*P.a.*) to dissect the different pathways for BALT induction and maturation. While MVA-induced BALT harbored CXCL13$^+$ FDCs in WT, *Il17a/f*$^{-/-}$, and *Myd88*$^{-/-}$*Trif*$^{-/-}$ mice, BALT induced by *P.a.* generally failed to develop FDCs and, within *Il17a/f*$^{-/-}$ and *Myd88*$^{-/-}$*Trif*$^{-/-}$ mice, showed an impaired morphological development and maturation.

Mechanistically, *P.a.* was found to induce, in an IL-17–dependent process, follicular stromal cells to express CXCL12 which enabled B cell recruitment and follicle formation in BALT even in the absence of FDCs. Furthermore, our study identified γδ T cells within BALT as a major source for IL-17, triggering the differentiation of stromal cells into podoplanin$^+$ (gp38) follicular cells that express CXCL12.

RESULTS AND DISCUSSION

P.a.-induced BALT depends on IL-17

We have recently shown that a single intranasal application of the replication-deficient MVA is sufficient to induce highly organized BALT (Halle et al., 2009), whereas others have reported that repetitive inhalations of heat-killed *P.a.* also lead to the development of BALT (Toyoshima et al., 2000). To gain

further insight into the role of IL-17 in BALT formation, we applied heat-inactivated *P.a.* (intranasally, on day 0 and day 6) to WT C57BL/6 (WT) and IL17a/f-deficient (*Il17a/f*$^{-/-}$) mice and compared the resulting BALT to that induced by a single intranasal application of MVA.

12 d after application of both *P.a.* and MVA, we observed BALT formation in WT mice, characterized by the presence of B cell follicles surrounded by T cell areas (Fig. 1 A). Interestingly, whereas MVA-induced BALT contained CXCL13^{+}CD21/CD35^{+} FDCs, BALT induced by *P.a.* was characterized by the absence of FDCs or other CXCL13-expressing cells (Fig. 1 B). We therefore analyzed the expression of other chemokines and identified the ligand for the chemokine receptor CXCR4 (Okada et al., 2002) in both MVA- and *P.a.*-induced BALT stromal cells (Fig. 1 C). Interestingly, *P.a.* failed to induce BALT in *Il17a/f*$^{-/-}$ mice. Lymphoid structures induced under these conditions lacked, to a large degree, organized B cell follicles, and B and T cells present were distributed throughout the structures (Fig. 1, D and E). Furthermore, CXCL12-expressing stromal cells were also largely absent (Fig. 1 F). In contrast, as reported before, MVA-induced BALT developed virtually identically in the lungs of WT and *Il17a/f*$^{-/-}$ mice, including the presence of CXCL13-expressing FDCs and CXCL12-expressing follicular stromal cells (Fig. 1 G). Of interest, CXCL12^{+} follicular stromal cells do not express CD21/CD35 and are thus different from FDCs (unpublished data). Because LT is known to drive FDC differentiation, we analyzed lung B cells from *P.a.*- or MVA-treated mice for the expression of LT$\alpha_1\beta_2$. Whereas LT$\alpha_1\beta_2$ was expressed on lung B cells of MVA-treated mice, it was not detectable on lung B cells of *P.a.*-treated mice (Fig. 1 H). These data indicate that distinct pathogens have different effects on LT$\alpha_1\beta_2$ expression that might also affect the development of FDCs and consequently of germinal centers. The absence of FDCs in *P.a.*-induced BALT was paralleled by impaired germinal center formation reflected by strongly reduced numbers of PNA^{+} B cells in *P.a.*-induced BALT (Fig. 1 I). Neither serum nor bronchoalveolar lavage antibody titers against the BALT-inducing pathogen showed significant differences for any of the isotypes tested (IgG1, IgG2b, IgG2c, IgM, and IgA; not depicted), but more CD138^{+}IgA^{+} plasma cells could be detected in MVA- than in *P.a.*-induced BALT (Fig. 1 J). Together, these findings indicate that FDCs present in BALT support local IgA class switch and that lymphoid organs other than BALT, such as bronchial lymph nodes, participate in the humoral immune response against BALT-inducing pathogens. Because lymphoid structures induced by *P.a.* in the lungs of *Il17a/f*$^{-/-}$ mice (and further gene targeted mice; see below) do not display the characteristic morphology of BALT, i.e., lacking segregated B cell follicles and T cell areas, we will refer to them as lymphoid aggregates throughout the manuscript.

Quantitative analysis of the number of lymphoid aggregates per lung section, the size of individual lymphoid aggregates, and the cumulated size of all lymphoid aggregates failed to reveal any differences between WT and *Il17a/f*$^{-/-}$ mice after MVA or *P.a.* exposure (Fig. 2, A–C). To further analyze and quantify the difference of *P.a.*-induced lymphoid tissue in WT and *Il17a/f*$^{-/-}$ mice, we classified all induced aggregates into three types based on the status of B cell distribution. Aggregates with densely packed B cell follicles and clearly segregated T cell zones (i.e., typical BALT) were classified as type I (Fig. 2 D, left). Lymphoid aggregates which failed to develop densely packed follicles but still contained numerous B cells were defined as type II aggregates (Fig. 2 D, middle), whereas all induced aggregates containing none or only very few B cells,

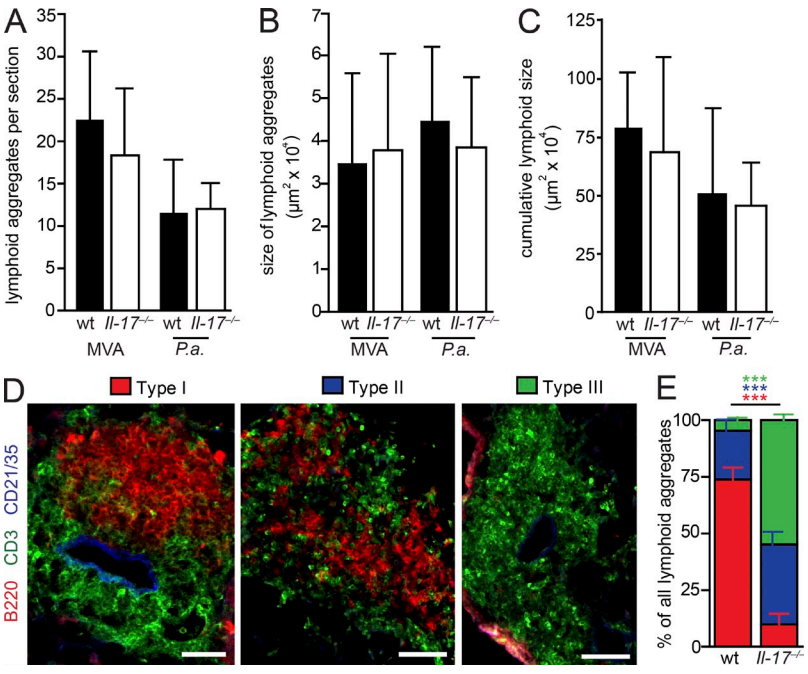

Figure 2. Formation of B cell follicles in *P.a.*-induced BALT requires IL-17. (A–C) Quantification of MVA-induced BALT in the lungs of WT (n = 16) and *Il17a/f*$^{-/-}$ (n = 7) mice as well as *P.a.*-induced BALT in the lungs of WT (n = 9) and *Il17a/f*$^{-/-}$ (n = 7) mice. Data are derived from at least two independent experiments; error bars represent mean ± SD. (A) Number of lymphoid aggregates/section. (B) Size of individual lymphoid aggregates. (C) Cumulative BALT size calculated as sum of all individual lymphoid structures per lung section. (D) Representative immunofluorescence micrographs of three different types (I, II, and III) of *P.a.*-induced BALT. Bars, 100 µm. (E) Relative frequency of *P.a.*-induced type I, type II, and type III BALT in lungs of WT (n = 9) and *Il17a/f*$^{-/-}$ (n = 7) mice. Data are derived from at least two independent experiments. Error bars indicate mean and SD; ***, $P < 0.001$, color of stars refers to the type of BALT as indicated.

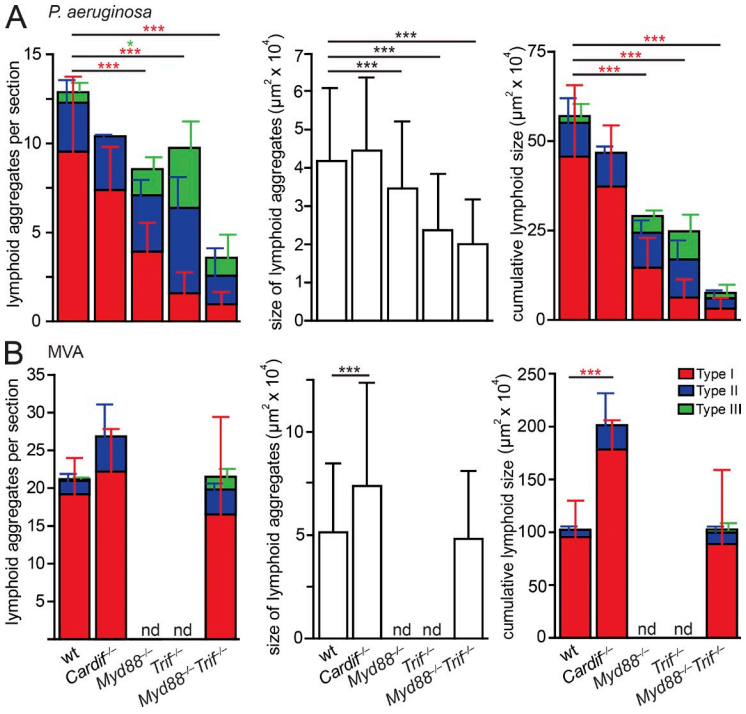

Figure 3. Additive effects of MyD88 and TRIF in *P.a.*-induced BALT. (A) Quantification of *P.a.*-induced BALT in the lungs of WT ($n = 9$), *Cardif*$^{-/-}$ ($n = 5$), *Myd88*$^{-/-}$ ($n = 5$), *Trif*$^{-/-}$ ($n = 6$), and *Myd88*$^{-/-}$*Trif*$^{-/-}$ ($n = 7$) mice. (B) Quantification of MVA-induced BALT in the lungs of WT ($n = 8$), *Cardif*$^{-/-}$ ($n = 5$), and *Myd88*$^{-/-}$*Trif*$^{-/-}$ ($n = 4$) mice. Cumulative BALT size (right) was calculated as the sum of all individual lymphoid structures per lung section. Data are derived from at least two independent experiments. Error bars indicate mean and SD; *, $P < 0.05$; ***, $P < 0.001$, gene-targeted versus WT; color of stars refers to the type of BALT as indicated.

but considerable amounts of T cells, were counted as type III aggregates (Fig. 2 D, right). The majority (~75%) of *P.a.*-induced lymphoid aggregates in WT mice belonged to type I, whereas only 10% of lymphoid structures in *Il17a/f*$^{-/-}$ mice met the criteria for this type. In contrast, <5% of lymphoid aggregates in WT mice were type III aggregates after *P.a.* exposition, but >50% of all aggregates in *Il17a/f*$^{-/-}$ mice belonged to this group (Fig. 2 E). Collectively, these data indicate that IL-17 signaling plays an essential role in the formation of B cell follicles in *P.a.*- but not MVA-induced BALT. Furthermore, MVA induces CXCL13^{+} FDCs as well as CXCL12-expressing follicular stromal cells, whereas application of *P.a.* does not allow for FDC differentiation and induces CXCL12^{+} stromal cells only in the presence of IL-17.

Additive effects of MyD88 and TRIF in *P.a.*-induced BALT

Recent studies have shown that TLRs are involved in the recognition of *P.a.* (Adamo et al., 2004) and that the two adaptor molecules MyD88 and TRIF divide TLR signaling pathways. Furthermore, caspase recruitment domain adaptor-inducing interferon-β (Cardif) is a crucial adaptor molecule in the signaling cascade of RIG-I–like receptors in antiviral responses such as against MVA (Delaloye et al., 2009). We therefore attempted to induce BALT in mice deficient for one (*Myd88*$^{-/-}$, *Trif*$^{-/-}$, or *Cardif*$^{-/-}$) or two (*Myd88*$^{-/-}$*Trif*$^{-/-}$) of these adaptors.

Although Cardif deficiency had no effect on *P.a.*-induced BALT, deficiency for MyD88 or TRIF affected the number, size, and type of lymphoid aggregates induced; structures were reduced in number and size, and B cells were both less frequent and aggregated. Interestingly, in *Myd88/Trif* double-deficient mice, these impairments were even more severe, suggesting additive effects of these signaling adaptors during BALT induction by *P.a.* (Fig. 3 A).

In contrast, MVA-induced lymphoid aggregates in *Myd88*$^{-/-}$*Trif*$^{-/-}$ mice were not significantly different from those of WT mice, whereas Cardif-deficient mice possessed aggregates that were even larger (Fig. 3 B), confirming a role for this adapter in the immune response to MVA infection. Because MVA is known to be sensed by a combination of multiple extra- and intracellular pattern recognition receptors, such as TLR2-TLR6 heterodimers, MDA-5 (melanoma differentiation-associated gene 5), and the NALP3 (NACHT, LRR, and PYD domains-containing protein 3) inflammasome (Delaloye et al., 2009), it seems plausible that singular defects in selected pathways can be compensated by others to still allow for the formation of highly organized MVA-induced BALT.

Interfering with CXCL12/CXCR4 signaling leads to impaired B cell follicle formation in *P.a.*-induced lymphoid tissue

We next addressed the functional role of CXCL12 in the development and maintenance of B cell follicles in *P.a.*-induced lymphoid aggregates. To this end, we injected neutralizing anti-CXCL12 antibodies i.p. at days 6 and 9 of *P.a.* BALT induction. This treatment strongly reduced the number of induced lymphoid aggregates (Fig. 4 A), whereas the individual size of the remaining aggregates was not significantly changed (not depicted). Only ~10% of the remaining lymphoid aggregates developed densely packed B cell follicles (type I aggregates), whereas the vast majority was of type II or III (Fig. 4 A). These findings suggest that CXCL12 plays a crucial role for the recruitment of B cells and the development and maintenance of B cell follicles within *P.a.*-induced BALT.

To further corroborate this hypothesis, we administered AMD3100, a competitive antagonist for CXCR4 (De Clercq, 2003), to WT mice during BALT induction by *P.a.* AMD3100 treatment resulted in a significant reduction of ectopic lymphoid tissue in the lungs regarding the number of lymphoid aggregates as well as their individual and cumulative size (Fig. 4 B and not depicted). Less than 25% of the lymphoid aggregates present met the criteria for type I aggregates, whereas the majority was characterized by loose infiltrates of T and B cells (Fig. 4 B). Collectively, these experiments demonstrate that the CXCL12–CXCR4 signaling pathway is essential for appropriate maturation of B cell follicles in *P.a.*-induced BALT. Interestingly, when testing for a role of CXCL12–CXCR4 in MVA-mediated BALT induction, we did not detect any differences between AMD3100- and PBS-treated WT mice, including the unchanged presence of FDCs (Fig. 4 C and not depicted). In contrast, treatment of CXCR5-deficient mice with AMD3100 led to a reduction in numbers and size of lymphoid aggregates, as well as of type I aggregate frequencies (Fig. 4 D).

These data suggest that both CXCL12 and CXCL13 contribute to the formation of B cell follicles in induced lymphoid tissue in the lung, and that some pathogens, such as MVA, induce both chemokines while others, such as *P.a.*, only induce CXCL12 in follicular stromal cells, a process which is dependent on IL-17. Importantly, in the presence of functional CXCR5 and CXCL13-expressing FDCs, CXCL12 is obviously not required for B cell recruitment and follicle formation in BALT. However, lymphoid structures induced by pathogens that fail to induce CXCL13-expressing FDCs, such as *P.a.*, can only mature into BALT with segregated B and T cell areas when the inducing agent triggers CXCL12 expression on stromal cells other than FDCs.

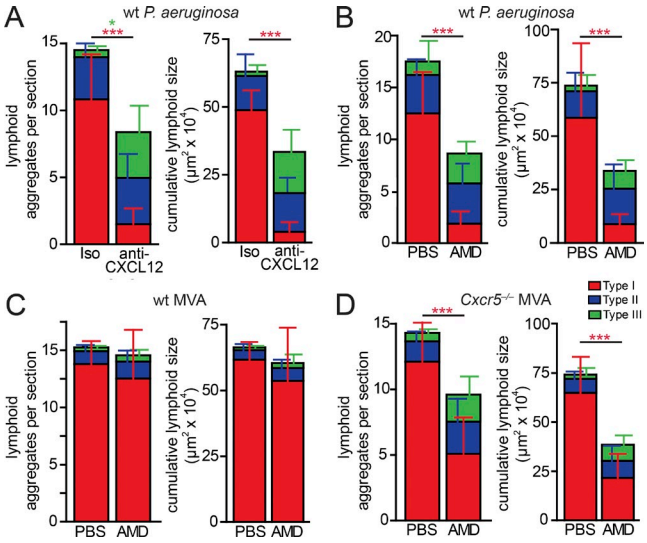

Figure 4. CXCL12/CXCR4 signaling is required for development of B cell follicles in *P.a.*-induced BALT. (A) Number of lymphoid aggregates per section and cumulative size of lymphoid structures per section of *P.a.*-induced BALT after i.p. treatment of WT mice with neutralizing anti-CXCL12 antibodies (anti-CXCL12; $n = 6$) or isotype control (Iso; $n = 5$; data are derived from three independent experiments). (B–D) Number of lymphoid aggregates per section and cumulative size of lymphoid structures per section of BALT induced in WT (B and C) or CXCR5$^{-/-}$ (D) mice after *P.a.* (B) or MVA (C and D) administration in the absence (PBS; $n = 4$–5) or presence (AMD; $n = 8$) of AMD3100. Data are derived from at least two independent experiments. Error bars indicate mean and SD; *, $P < 0.05$; ***, $P < 0.001$; color of stars refers to the type of BALT as indicated.

Up-regulation of CXCL12 expression in pulmonary stromal cells by IL-17

To confirm the hypothesis that IL-17 promotes the expression of CXCL12, pulmonary stromal cells were isolated from WT mice and cultured for various periods of time in the presence or absence of recombinant IL-17. In a time-dependent manner, IL-17 treatment resulted in increased production of CXCL12 as determined by ELISA (Fig. 5 A). Podoplanin$^+$CD31$^-$ stromal cells could be identified as the major source of CXCL12 at all tested time points (Fig. 5 B). Furthermore, immunofluorescence microscopy of cultured pulmonary stromal cells revealed heterogeneous expression of CXCL12 after stimulation with IL-17. A considerable proportion of stromal cells expressed CXCL12 at high levels but CXCL12^{low} cells were also present (Fig. 5 C). Interestingly, many CXCL12-expressing cells co-expressed podoplanin (Fig. 5 C) but were negative for CD31, a marker for vascular endothelial cells, or CD21/35, a marker for FDCs (not depicted). This expression profile is characteristic for fibroblastic reticular cells (FRCs) present in lymph nodes, suggesting that podoplanin$^+$ CD31$^-$CD21/35$^-$ FRC-like pulmonary stromal cells are a source of CXCL12 in induced BALT. Indeed, immunohistological analysis of *P.a.*-induced lymphoid aggregates in the lung revealed that CXCL12 is expressed by many podoplanin$^+$ stromal cells (Fig. 5 D) but also by cells lacking podoplanin expression.

Given that IL-17 signaling promotes the expression of CXCL12 on pulmonary stromal cells, we further investigated the influence of γδ T cells, which have been shown to be a potent source of IL-17 in the lung (Lockhart et al., 2006). To this end, we treated γδ T cell–deficient (*Tcrd*$^{-/-}$) mice intranasally with *P.a.* and found a BALT phenotype similar to that of *Il17a/f*$^{-/-}$ mice, including a reduced frequency of type I aggregates (Fig. 5 E). In contrast to IL-17–deficient mice BALT induced by *P.a.* in *Tcrd*$^{-/-}$ mice was less frequently present and smaller in cumulative size when compared with WT mice indicating that γδ T cells have other roles in BALT formation in addition to IL-17 production. We then analyzed *P.a.*-induced lymphoid aggregates in reporter mice harboring γδ T cells with a green fluorescent nucleus (*TcrdH2BeGFP* mice). Few γδ T cells were already present within areas of infiltrating T and B cells at day 4 of BALT induction, whereas clusters of γδ T cells appeared at day 7 and were abundantly present in mature aggregates at day 12 (Fig. 5 F). Hardly any γδ T cells were found outside lymphoid aggregates but were also present in MVA-induced BALT (Fig. 5 F and not depicted). Flow cytometry from cells isolated from the lungs at day 12 of *P.a.*-treated mice revealed that γδ T cells were present

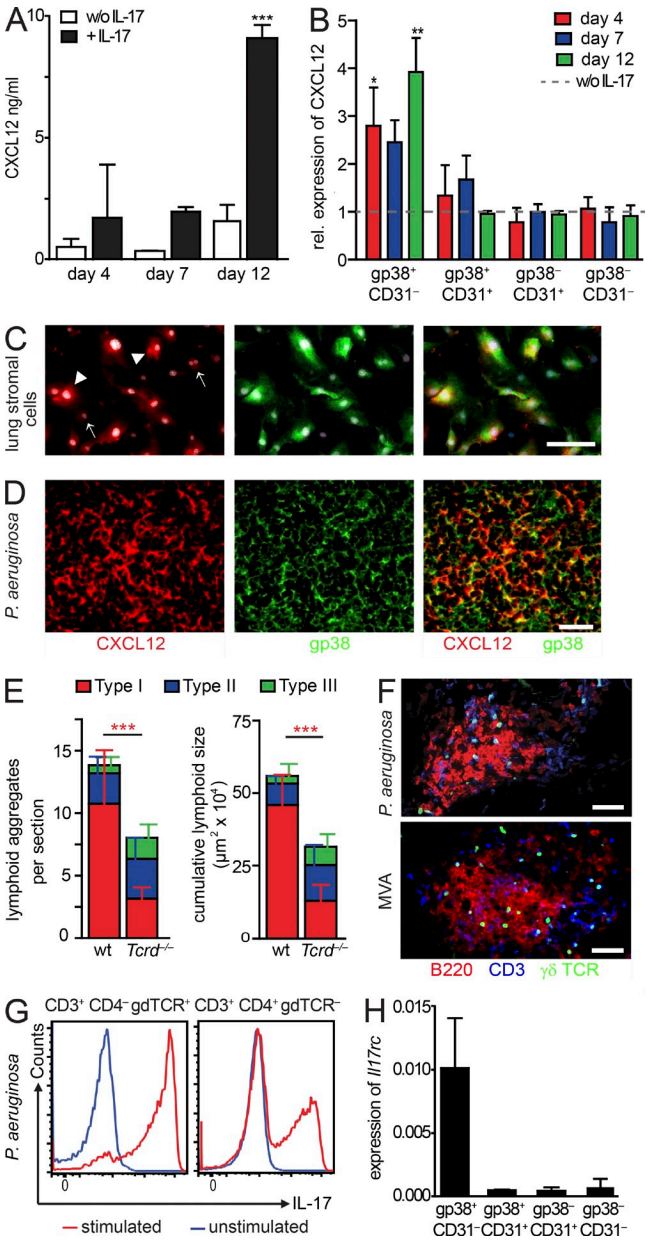

Figure 5. IL-17 induces CXCL12 expression of pulmonary stromal cells. (A and B) Pulmonary stromal cells were isolated and cultured in the absence or presence of 100 ng/ml murine IL-17 for 4, 7, or 12 d. (A) CXCL12 production determined by ELISA at the time point indicated. Data are derived from three independent experiments with duplicate cultures. Error bars indicate mean and SD; ***, $P < 0.001$. (B) CD45$^-$ cultured stromal cells were sorted at days 4, 7, and 12 of culture according to their gp38 and CD31 expression as indicated. Relative expression levels of CXCL12 normalized to *Gapdh* determined by qRT-PCR in duplicates. Expression of CXCL12 in the absence of IL-17 has been set to 1 for each point of time and cell population analyzed (dashed line). Data are derived from two independent experiments. Error bars indicate mean and SD; *, $P < 0.05$; **, $P < 0.01$, versus without IL-17. (C and D) Immunofluorescence of pulmonary stromal cells grown for 12 d on adhesive slides in the presence of IL-17 (C) and BALT sections 12 d after intranasal application of *P.a.* (D) Red, anti-CXCL12 (left); green, anti-podoplanin (middle); merge (right). Arrowheads indicate CXCL12^{high} cells, and arrows indicate CXCL12^{low} cells. Images are representative of at least three independent experiments. Bars, 100 µm. (E) Quantification of *P.a.*-induced BALT in the lungs of WT ($n = 9$) and *Tcrd* $^{-/-}$ ($n = 8$) mice. Data are derived from three independent experiments. Mean and SD; ***, $P < 0.001$, color of stars refers to the type of BALT as indicated. (F) Immunofluorescence microscopy of *P.a.*-induced (top) and MVA-induced BALT (bottom) in *TcrdH2BeGFP* mice 12 d after i.n. administration; red, anti-B220; blue, anti-CD3; green, γδ T cells. Bars, 100 µm. Images are representative for 4–5 mice analyzed in two independent experiments. (G) IL-17 expression on T cell subpopulations isolated from lungs of WT mice 12 d after i.n. administration of *P.a.* For intracellular IL-17 staining, cells were either stimulated with PMA/ionomycin or left unstimulated. Data are representative for three independent experiments with $n = 8$ mice analyzed. (H) Freshly isolated CD45$^-$ pulmonary stromal cells were sorted according to CD31 and gp38 expression in groups as indicated. Expression levels of *Il17rc* normalized to *Gapdh* were determined by qRT-PCR in duplicates. Data are derived from two independent experiments; mean and SD.

at higher frequencies in *P.a.*- than in MVA-induced BALT (9.50 ± 4.4% of all leukocytes vs. 5.85 ± 0.7%, mean and SD) and that >70% of γδ T cells expressed IL-17 at high levels, whereas only few CD4$^+$ T cells expressed low levels of this cytokine (Fig. 5 G). Because IL-17$^+$ γδ T cells were amply present in B cell follicles that contain CXCL12-producing cells, we asked if IL-17 could potentially have a direct effect on these cells. Indeed, quantitative RT-PCR on freshly isolated stromal cells revealed that podoplanin (gp38)$^+$CD31$^-$ FRC-like cells express high levels of IL-17Rc (Fig. 5 H). Together, these data indicate that IL-17, primarily produced by γδ T cells in the lung, allows for the activation of IL-17Rc$^+$podoplanin$^+$ pulmonary stromal cells to express CXCL12. This chemokine then leads to recruitment of B cells and follicle formation in BALT induced by pathogens which, such as *P.a.*, lack the capacity to induce FDCs.

This study identifies two different pathways for pathogen-induced BALT formation: MVA-induced BALT contains FDCs as well as CXCL12$^+$ follicular stromal cells while *P.a.*-induced BALT lacks FDCs but contains CXCL12$^+$ stromal cells. The latter allows B cell recruitment and follicle formation via B cell–expressed CXCR4 even in the absence of CXCL13-positive FDCs recruiting B cells via CXCR5. We also tested for a potential role for CCL21, a ligand for CCR7, in follicle formation of *P.a.*-induced BALT. In contrast to CXCL12 and CXCL13, CCL21 was found on HEVs but not in B cell follicles (unpublished data). This observation, together with our earlier findings that CCR7-deficient mice develop BALT spontaneously (Kocks et al., 2007), argues against a role for CCR7 in the formation of follicles in BALT. The finding that IL-17 plays an important role for the differentiation of lung stromal cells (as well as potentially other cells) to CXCL12-expressing follicular stromal cells, a step essential for BALT formation in the absence of FDCs, provides novel insights on the differential requirement for IL-17 in BALT induction reported earlier (Rangel-Moreno et al., 2011; Fleige et al., 2012). We have recently shown that MVA-induced BALT acts as a general priming site for the initiation

of adaptive immune responses, not only against the BALT-inducing pathogen but also against unrelated antigens (Halle et al., 2009). As previously reported by others (Rangel-Moreno et al., 2007), we also observed largely unaffected antibody class switch in FDC-less BALT. Given that ectopic lymphoid tissues are commonly assumed to play a crucial role in the pathogenesis of autoimmune diseases such as diabetes or rheumatoid arthritis, IL-17 targeting approaches might allow for interference with tertiary lymphoid tissue development, at least in situations where FDCs are not involved. The differential role of IL-17 in ectopic lymphoid tissue formation might also help to explain why some autoimmune patients benefit more than others from anti–IL-17 treatment (Patel et al., 2013).

MATERIALS AND METHODS

Mice. Mice were bred at a local animal facility or purchased from Charles River. *Il-17a/f*$^{-/-}$ mice (Haas et al., 2012), *Blr1*$^{-/-}$ (CXCR5-deficient) mice (Förster et al., 1996), Cardif-deficient (*Cardif*$^{-/-}$) mice (Michallet et al., 2008), MyD88-deficient (MyD88$^{-/-}$) mice (Adachi et al., 1998), TRIF-deficient (*Trif*$^{-/-}$) mice (Hoebe et al., 2003), MyD88/TRIF double-knockout (*Myd88*$^{-/-}$*Trif*$^{-/-}$) mice (Waibler et al., 2009), *Tcrd*$^{-/-}$ mice (Itohara et al., 1993), and *TcrdH2BeGFP* mice (Prinz et al., 2006) have been described previously. All animals were maintained under SPF conditions and used at the age of 8–12 wk. All animal experiments have been performed in accordance with institutional guidelines and have been approved by the Niedersächsisches Landesamt für Verbraucherschutz und Lebensmittelsicherheit.

MVA. Clonal virus isolate F6 at passage 584 on primary chicken embryo fibroblasts (CEFs) was used for this study. Recombinant MVA constructs have been described previously and virus stocks were generated by standard methods (Sutter and Moss, 1992; Kremer et al., 2012). In brief, viruses were propagated on CEF, concentrated and purified by ultracentrifugation through sucrose, and titrated on CEF to determine infectious units (IU). Mice were deeply anesthetized with ketamine/xylazine, and 10^7 IU MVA diluted in 40 µl PBS was applied to the nostrils.

P.a. *P.a.* strain PA14 (Liberati et al., 2006) was routinely cultured at 37°C in Luria broth (LB) medium. The bacteria were adjusted to 5×10^9 CFU/ml in PBS and were heat-killed at 55°C for 60 min and autoclaving at 121°C for 90 min. For intranasal administration, mice were deeply anesthetized with ketamine/xylazine, and 10 µl of a 5×10^9 CFU/ml *P.a.* stock was diluted in 40 µl PBS.

Antibody treatment. For blocking assays, 250 µg neutralizing anti–human/mouse CXCL12 (clone 79014; R&D Systems) or mouse IgG1 isotype control Ab was intraperitoneally injected at days 6 and 9 after intranasal application of *P.a.* Mice were analyzed at day 12.

In vivo AMD3100 treatment. To ensure sufficient levels of the antagonist throughout the 12-d experimental period, we used osmotic minipumps (Model 2002; Alzet) to deliver AMD3100 (Sigma-Aldrich) at a constant rate of 250 µg/kg/h. The pumps loaded with AMD3100 diluted in PBS or only PBS were implanted dorsolaterally under the skin of WT or CXCR5$^{-/-}$ mice. All mice were anesthetized with ketamine/xylazine. Osmotic pumps were implanted on day 0 simultaneously with intranasal administration of either MVA or *P.a.*

Immunohistology. For immunohistology, mice were perfused with 5 ml of ice-cold PBS, and the lung was filled with a 1:1 mixture of Tissue-Tek OCT (Sakura) and PBS via the trachea, embedded in OCT, and frozen on dry ice. 8-µm sections were performed with a cryostat (CM3050; Leica) and fixed for 10 min in ice-cold acetone. Cryosections were rehydrated in Tris-buffered saline with 0.05% Tween 20, blocked with 5% mouse or rat serum, and stained with the following antibodies at room temperature for 45 min: B220-Cy3 (RA3-GB2), CD3-Cy5 (17A2; all prepared in-house), CD21/35-FITC (7G6; BD), and podoplanin/gp38-biotin (8.1.1; eBioscience) detected with streptavidin-Cy3. Chemokine staining was performed by using a Tyramide Signal Amplification (TSA) Cyanine 3 system (PerkinElmer). The following antibodies were used: goat anti-CXCL13 (AF 470; R&D Systems) and goat anti-CXCL12 (PeproTech) detected with donkey anti–goat HRP (Jackson ImmunoResearch Laboratories, Inc.).

Stromal cells, isolated from the lung, were grown for 10–12 d on Histo-Bond cover slides, air dried, acetone-fixed for 10 min, and stained with the following antibodies: podoplanin-biotin (8.1.1; eBioscience), goat anti-CXCL12 (PeproTech), and the secondary antibodies donkey anti–goat HRP and streptavidin Cy3 (Jackson ImmunoResearch Laboratories, Inc.). Immunohistological analysis of the lung was performed at room temperature using a motorized epifluorescence microscope (BX61; UPlanSApo objectives: 10×/0.4, 20×/0.75, and 40×/0.9) equipped with a fluorescence camera (F-View II) and cellSens software (all from Olympus).

Quantification of BALT. The amount of BALT was quantified as follows: whole central sections of four different areas (close to main bronchi and vessels) per lung/mice were analyzed. Individual BALT structures were counted and measured, and the cumulative lymphoid size was calculated as the sum of all individual lymphoid structures present on one central lung section (polygon tool, cellSens software; Olympus). For categorization of induced lymphoid aggregates, we assigned all lymphoid aggregates to three types based on their B cell status and calculated the means of lymphoid aggregates per section and the means of cumulative lymphoid size for all three types.

Isolation and culture of primary pulmonary stromal cells. Lungs from 8–12-wk-old mice were digested using liberase and DNase I (both from Roche), filtered through a 100-µm cell strainer and single-cell suspensions were cultured overnight in DMEM substituted with 10% FCS, 1% penicillin and streptomycin, 400 µl/liter gentamycin, and 3.5 µl/liter β-mercaptoethanol. Non-adherent cells were removed the next day, and after 3 d fresh medium was added to the remaining cells. Adherent cells were grown for an additional 3 d and were then treated for 4, 7, or 12 d with 100 ng/ml IL-17 (PeproTech). For cell sorting, either freshly isolated or cultured CD45$^-$ stromal cells were sorted according to podoplanin (gp38) and CD31 expression into four fractions: gp38$^+$CD31$^-$, gp38$^+$CD31$^+$, gp38$^-$CD31$^+$, and gp38$^-$CD31$^-$.

RNA extraction and quantitative RT-PCR. Cells were harvested and total RNA was extracted by using an RNeasy Plus Mini kit (QIAGEN). cDNA was prepared with Superscript III and random hexamer primers (Invitrogen). Quantitative RT-PCR was performed using the SYBR Premix EX Taq (Takara Bio Inc.) on a LightCycler machine (Roche). Expression levels were measured using the following primers: *Cxcl12* forward, 5′-GAGAGCCACATCGCCAGAG-3′, reverse, 5′-TTTCGGGTCAATGCACACTTG-3′; *Il17rc* forward, 5′-GAGTCCCTGCCAGCCACTT-3′, reverse, 5′-ACTGGAAATCTTGTGGCTCC-3′; and *Gapdh* forward, 5′-GTGCCAGCCTCGTCCCGTAG-3′, reverse, 5′-TTGCCGTGAGTGGAGTCATAC-3′. Relative expression levels were calculated by normalizing CXCL12 or IL-17Rc levels to *Gapdh* and using the $2^{-\Delta\Delta Ct}$ method.

ELISA. Concentration of CXCL12 in supernatants of cultured pulmonary stromal cells was measured by sandwich ELISA using mouse CXCL12α Quantikine ELISA kit (R&D Systems). An automated microplate reader set at 450 nm was used to measure OD. The mean minimum detectable dose for CXCL12 was 0.044 ng/ml. A calibration standard ranging from 0.156 to 10 ng/ml was used to draw a standard curve by plotting OD versus the concentration of CXCL12.

Flow cytometry and intracellular cytokine staining. Lungs were perfused with PBS, cut into small pieces, and digested with 0.5 mg/ml collagenase

D and 0.025 mg/ml DNase I in RPMI 1640 with 5% FCS and 25 mM Hepes for 45 min at 37°C, followed by enzymatic inactivation by adding 20 mM EDTA. Digested lungs were mashed through a 40-µm cell strainer (Thermo Fisher Scientific) with RPMI 1640 5% FCS. Lymphocytes were obtained from the resulting single cell suspension by density gradient centrifugation with Lympholyte M. To detect surface expression of $LT\alpha_1\beta_2$, cells were pretreated with blocking anti-FcR mAb (2.4.G2). LTβR-Ig (Krege et al., 2009) was added and detected using goat anti–human IgG-PE (Jackson, ImmunoResearch Laboratories, Inc.).

For measurement of intracellular IL-17, lymphocytes were restimulated with 50 ng/ml PMA (EMD Millipore) and 2 µg/ml ionomycin (Invitrogen) in the presence of brefeldin A (Sigma-Aldrich) for 4 h. Cells were fixed using the Cytofix/Cytoperm kit (BD) as described in the supplier's manual. FACS analysis was performed using a LSRII flow cytometer (BD) and FACS sorting was performed on a FACSAria IIU (BD). The following antibodies were used: CD45 (clone 104), podoplanin (clone 8.1.1), CD31 (clone Mec 13.3), B220 (clone RA3-GB2), CD3 (clone 17A2), CD4 (clone RM4-5), αβ-TCR (clone H57-597), TCR-γδ (clone GL3), and IL-17A (clone ebio17B7).

Statistical analysis. Statistical analysis was performed with Prism 4 (GraphPad Software, Inc.). All significant values were determined using unpaired two-tailed Student's *t* test or one-way ANOVA.

We are grateful to Ralph Scherer for help with statistical analysis. We thank Mathias Herberg for excellent animal care, Barbara Köttgen for expert technical assistance, and Tim Worbs for critical review of the manuscript.

This work was supported by Deutsche Forschungsgemeinschaft (DFG) grants SFB587-B3 and SFB900-B1 to R. Förster and SFB900-A3 to S. Häussler, the Hannover Biomedical Research School (HBRS), and the Center for Infection Biology (ZIB).

The authors declare no competing financial interests.

Submitted: 19 August 2013
Accepted: 4 March 2014

REFERENCES

Adachi, O., T. Kawai, K. Takeda, M. Matsumoto, H. Tsutsui, M. Sakagami, K. Nakanishi, and S. Akira. 1998. Targeted disruption of the MyD88 gene results in loss of IL-1- and IL-18-mediated function. *Immunity*. 9:143–150. http://dx.doi.org/10.1016/S1074-7613(00)80596-8

Adamo, R., S. Sokol, G. Soong, M.I. Gomez, and A. Prince. 2004. *Pseudomonas aeruginosa* flagella activate airway epithelial cells through asialoGM1 and toll-like receptor 2 as well as toll-like receptor 5. *Am. J. Respir. Cell Mol. Biol.* 30:627–634. http://dx.doi.org/10.1165/rcmb.2003-0260OC

De Clercq, E. 2003. The bicyclam AMD3100 story. *Nat. Rev. Drug Discov.* 2:581–587. http://dx.doi.org/10.1038/nrd1134

Delaloye, J., T. Roger, Q.G. Steiner-Tardivel, D. Le Roy, M. Knaup Reymond, S. Akira, V. Petrilli, C.E. Gomez, B. Perdiguero, J. Tschopp, et al. 2009. Innate immune sensing of modified vaccinia virus Ankara (MVA) is mediated by TLR2-TLR6, MDA-5 and the NALP3 inflammasome. *PLoS Pathog.* 5:e1000480. http://dx.doi.org/10.1371/journal.ppat.1000480

Fleige, H., J.D. Haas, F.R. Stahl, S. Willenzon, I. Prinz, and R. Förster. 2012. Induction of BALT in the absence of IL-17. *Nat. Immunol.* 13:1, author reply :2. http://dx.doi.org/10.1038/ni.2167

Förster, R., A.E. Mattis, E. Kremmer, E. Wolf, G. Brem, and M. Lipp. 1996. A putative chemokine receptor, BLR1, directs B cell migration to defined lymphoid organs and specific anatomic compartments of the spleen. *Cell*. 87:1037–1047. http://dx.doi.org/10.1016/S0092-8674(00)81798-5

GeurtsvanKessel, C.H., M.A. Willart, I.M. Bergen, L.S. van Rijt, F. Muskens, D. Elewaut, A.D. Osterhaus, R. Hendriks, G.F. Rimmelzwaan, and B.N. Lambrecht. 2009. Dendritic cells are crucial for maintenance of tertiary lymphoid structures in the lung of influenza virus–infected mice. *J. Exp. Med.* 206:2339–2349. http://dx.doi.org/10.1084/jem.20090410

Haas, J.D., S. Ravens, S. Düber, I. Sandrock, L. Oberdörfer, E. Kashani, V. Chennupati, L. Föhse, R. Naumann, S. Weiss, et al. 2012. Development of interleukin-17-producing γδ T cells is restricted to a functional embryonic wave. *Immunity*. 37:48–59. http://dx.doi.org/10.1016/j.immuni.2012.06.003

Halle, S., H.C. Dujardin, N. Bakocevic, H. Fleige, H. Danzer, S. Willenzon, Y. Suezer, G. Hämmerling, N. Garbi, G. Sutter, et al. 2009. Induced bronchus-associated lymphoid tissue serves as a general priming site for T cells and is maintained by dendritic cells. *J. Exp. Med.* 206:2593–2601. http://dx.doi.org/10.1084/jem.20091472

Hoebe, K., X. Du, P. Georgel, E. Janssen, K. Tabeta, S.O. Kim, J. Goode, P. Lin, N. Mann, S. Mudd, et al. 2003. Identification of Lps2 as a key transducer of MyD88-independent TIR signalling. *Nature*. 424:743–748. http://dx.doi.org/10.1038/nature01889

Itohara, S., P. Mombaerts, J. Lafaille, J. Iacomini, A. Nelson, A.R. Clarke, M.L. Hooper, A. Farr, and S. Tonegawa. 1993. T cell receptor δ gene mutant mice: independent generation of αβ T cells and programmed rearrangements of γδ TCR genes. *Cell*. 72:337–348. http://dx.doi.org/10.1016/0092-8674(93)90112-4

Kahnert, A., U.E. Höpken, M. Stein, S. Bandermann, M. Lipp, and S.H. Kaufmann. 2007. *Mycobacterium tuberculosis* triggers formation of lymphoid structure in murine lungs. *J. Infect. Dis.* 195:46–54. http://dx.doi.org/10.1086/508894

Kocks, J.R., A.C. Davalos-Misslitz, G. Hintzen, L. Ohl, and R. Förster. 2007. Regulatory T cells interfere with the development of bronchus-associated lymphoid tissue. *J. Exp. Med.* 204:723–734. http://dx.doi.org/10.1084/jem.20061424

Kocks, J.R., H. Adler, H. Danzer, K. Hoffmann, D. Jonigk, U. Lehmann, and R. Förster. 2009. Chemokine receptor CCR7 contributes to a rapid and efficient clearance of lytic murine γ-herpes virus 68 from the lung, whereas bronchus-associated lymphoid tissue harbors virus during latency. *J. Immunol.* 182:6861–6869. http://dx.doi.org/10.4049/jimmunol.0801826

Krege, J., S. Seth, S. Hardtke, A.C. Davalos-Misslitz, and R. Förster. 2009. Antigen-dependent rescue of nose-associated lymphoid tissue (NALT) development independent of LTβR and CXCR5 signaling. *Eur. J. Immunol.* 39:2765–2778. http://dx.doi.org/10.1002/eji.200939422

Kremer, M., A. Volz, J.H. Kreijtz, R. Fux, M.H. Lehmann, and G. Sutter. 2012. Easy and efficient protocols for working with recombinant vaccinia virus MVA. *Methods Mol. Biol.* 890:59–92. http://dx.doi.org/10.1007/978-1-61779-876-4_4

Liberati, N.T., J.M. Urbach, S. Miyata, D.G. Lee, E. Drenkard, G. Wu, J. Villanueva, T. Wei, and F.M. Ausubel. 2006. An ordered, nonredundant library of *Pseudomonas aeruginosa* strain PA14 transposon insertion mutants. *Proc. Natl. Acad. Sci. USA*. 103:2833–2838. http://dx.doi.org/10.1073/pnas.0511100103

Lockhart, E., A.M. Green, and J.L. Flynn. 2006. IL-17 production is dominated by γδ T cells rather than CD4 T cells during *Mycobacterium tuberculosis* infection. *J. Immunol.* 177:4662–4669.

Michallet, M.C., E. Meylan, M.A. Ermolaeva, J. Vazquez, M. Rebsamen, J. Curran, H. Poeck, M. Bscheider, G. Hartmann, M. König, et al. 2008. TRADD protein is an essential component of the RIG-like helicase antiviral pathway. *Immunity*. 28:651–661. http://dx.doi.org/10.1016/j.immuni.2008.03.013

Moyron-Quiroz, J.E., J. Rangel-Moreno, K. Kusser, L. Hartson, F. Sprague, S. Goodrich, D.L. Woodland, F.E. Lund, and T.D. Randall. 2004. Role of inducible bronchus associated lymphoid tissue (iBALT) in respiratory immunity. *Nat. Med.* 10:927–934. http://dx.doi.org/10.1038/nm1091

Okada, T., V.N. Ngo, E.H. Ekland, R. Förster, M. Lipp, D.R. Littman, and J.G. Cyster. 2002. Chemokine requirements for B cell entry to lymph nodes and Peyer's patches. *J. Exp. Med.* 196:65–75. http://dx.doi.org/10.1084/jem.20020201

Patel, D.D., D.M. Lee, F. Kolbinger, and C. Antoni. 2013. Effect of IL-17A blockade with secukinumab in autoimmune diseases. *Ann. Rheum. Dis.* 72:iii116–iii123. http://dx.doi.org/10.1136/annrheumdis-2012-202371

Prinz, I., A. Sansoni, A. Kissenpfennig, L. Ardouin, M. Malissen, and B. Malissen. 2006. Visualization of the earliest steps of γδ T cell development in the adult thymus. *Nat. Immunol.* 7:995–1003. http://dx.doi.org/10.1038/ni1371

Randall, T.D. 2010. Bronchus-associated lymphoid tissue (BALT) structure and function. *Adv. Immunol.* 107:187–241. http://dx.doi.org/10.1016/B978-0-12-381300-8.00007-1

Rangel-Moreno, J., J.E. Moyron-Quiroz, L. Hartson, K. Kusser, and T.D. Randall. 2007. Pulmonary expression of CXC chemokine ligand 13, CC

chemokine ligand 19, and CC chemokine ligand 21 is essential for local immunity to influenza. *Proc. Natl. Acad. Sci. USA*. 104:10577–10582. http://dx.doi.org/10.1073/pnas.0700591104

Rangel-Moreno, J., D.M. Carragher, M. de la Luz Garcia-Hernandez, J.Y. Hwang, K. Kusser, L. Hartson, J.K. Kolls, S.A. Khader, and T.D. Randall. 2011. The development of inducible bronchus-associated lymphoid tissue depends on IL-17. *Nat. Immunol.* 12:639–646. http://dx.doi.org/10.1038/ni.2053

Sutter, G., and B. Moss. 1992. Nonreplicating vaccinia vector efficiently expresses recombinant genes. *Proc. Natl. Acad. Sci. USA*. 89:10847–10851. http://dx.doi.org/10.1073/pnas.89.22.10847

Toyoshima, M., K. Chida, and A. Sato. 2000. Antigen uptake and subsequent cell kinetics in bronchus-associated lymphoid tissue. *Respirology*. 5:141–145. http://dx.doi.org/10.1046/j.1440-1843.2000.00241.x

van de Pavert, S.A., and R.E. Mebius. 2010. New insights into the development of lymphoid tissues. *Nat. Rev. Immunol.* 10:664–674. http://dx.doi.org/10.1038/nri2832

Waibler, Z., M. Anzaghe, T. Frenz, A. Schwantes, C. Pöhlmann, H. Ludwig, M. Palomo-Otero, A. Alcamí, G. Sutter, and U. Kalinke. 2009. Vaccinia virus-mediated inhibition of type I interferon responses is a multifactorial process involving the soluble type I interferon receptor B18 and intracellular components. *J. Virol.* 83:1563–1571. http://dx.doi.org/10.1128/JVI.01617-08

Xu, B., N. Wagner, L.N. Pham, V. Magno, Z. Shan, E.C. Butcher, and S.A. Michie. 2003. Lymphocyte homing to bronchus-associated lymphoid tissue (BALT) is mediated by L-selectin/PNAd, $\alpha_4\beta_1$ integrin/VCAM-1, and LFA-1 adhesion pathways. *J. Exp. Med.* 197:1255–1267. http://dx.doi.org/10.1084/jem.20010685